Langmuir
Article
pubs.acs.org/Langmuir

Redox-Active Concanavalin A: Synthesis, Characterization, and Recognition-Driven Assembly of Interfacial Architectures for Bioelectronic Applications

Diego Pallarola,[†,||] Nuria Queralto,[‡] Wolfgang Knoll,[§] Marcelo Ceolín,[†] Omar Azzaroni,*[,†] and Fernando Battaglini[||]

[†]*Instituto de Investigaciones Fisicoquímicas Teóricas y Aplicadas (INIFTA), Departamento de Química, Facultad de Ciencias Exactas, Universidad Nacional de La Plata, CONICET, CC 16 Suc. 4 (1900) La Plata, Argentina,* [‡]*Max-Planck-Institut für Polymerforschung, Ackermannweg 10 (55128) Mainz, Germany,* [§]*Austrian Institute of Technology (AIT), Donau-City-Strasse 1, (1220) Vienna, Austria, and* [||]*INQUIMAE, Departamento de Química Inorgánica, Analítica y Química Física, Facultad de Ciencias Exactas y Naturales, Universidad de Buenos Aires, Ciudad Universitaria, Pabellón 2, C1428EHA Buenos Aires, Argentina*

Received February 1, 2010. Revised Manuscript Received June 28, 2010

The convergence of chemistry, biology, and materials science has paved the way to the emergence of hybrid nanobuilding blocks that incorporate the highly selective recognition properties of biomolecules, with the tailorable functional capabilities of inorganic molecules. In this work, we describe for the first time the decoration of concanavalin A (Con A), a protein with the ability to recognize sugars and form glycoconjugates, with Os(II) redox-active complexes. This strategy enabled the construction of electroactive biosupramolecular materials whose redox potentials could be easily modulated through the facile molecular modification of the electroactive inorganic complexes. Small-angle X-ray scattering (SAXS), steady-state fluorescence, surface plasmon resonance (SPR) spectroscopy, matrix-assisted laser desorption/ionization-time-of-flight mass spectrometry (MALDI-TOF-MS), and differential-pulsed (DPV) and cyclic voltammetry (CV) were used to characterize the structural and functional features of the synthesized biohybrid building blocks as well as their respective supramolecular assemblies built up on gold electrodes. By harnessing the electroactive and carbohydrate-recognition properties of these tailor-made biohybrid building blocks, we were able to integrate glucose oxidase (GOx) onto gold electrodes via sugar−lectin interactions. The redox activity of the Os-modified Con A interlayer allowed the electronic connection between the multilayered GOx assemblies and the metal electrode as evidenced by the well-defined bioelectrocatalytic response exhibited by the biomolecular assemblies in the presence of the glucose in solution. We consider that this approach based on the spontaneous formation of redox-active biosupramolecular assemblies driven by recognition processes can be of practical relevance for the facile design of biosensors, as well as for the construction of new multifunctional bioelectrochemical systems.

Introduction

In recent years, the scientific community has witnessed a great deal of interest in the rational design of self-assembling building blocks constituted of hybrid bioinorganic entities.[1] The main motivation leading to the growing activity in this field stems from the possibility of merging the unique properties of the two classes of building blocks: fully "abiotic" molecules enabling exquisite control over a myriad of functional features and biomolecules displaying unique recognition properties. In particular, derivatization of naturally occurring proteins with artificial functional molecules represents one of the most promising approaches for the development of these tailor-made functional building blocks.[2] The incorporation of "abiotic" entities can confer versatile functions upon native proteins, which could have potential applications in diverse technological fields. Along these lines, the development of new interfaces connecting electronic devices and biological systems continues to receive tremendous attention within the ever-growing research area of nanobiotechnology.[3] Full electrical integration of specific biomolecules into bioelectronic platforms requires the design of building blocks which can mediate the electrical signal arising from any specific biochemical stimuli without altering the inherent biological functions of the chosen biomolecules. This represents the cornerstone of biofunctional systems and constitutes a key aspect to engineering biochemical motifs, interfaces to existing biological networks, or biochemical logic circuits, just to name a few examples.[4] Furthermore, the application of redox-active biomolecules, or extrinsically electroactive biomolecules, is gaining increasing relevance in materials science. This originates from the use of electrochemistry as a simple readout system capable of translating very specific biorecognition events into an electronic signal.[5] Many of the electrochemical strategies are based on the analysis of the electrochemical response of an electroactive label linked to the biomolecule, thus acting as a reporter of any particular biomolecular process. The necessity to incorporate electroactive centers into the biomolecule is required, because in most cases, the biomolecules displaying the desired molecular recognition properties are not intrinsically electroactive. Hence, in order to render them electroactive they are

*E-mail: azzaroni@inifta.unlp.edu.ar (O.A.) Homepage: http://softmatter.quimica.unlp.edu.ar.

(1) *Nanobiotechnology II: More Concepts and Applications*, Mirkin, C. A., Niemeyer, C. M., Eds.; VCH-Wiley: Weinheim, 2007.

(2) Katz, E.; Willner, I. in *Nanobiotechnology: Concepts, Applications and Perspectives*, Mirkin, C. A., Niemeyer, C. M., Eds.; VCH-Wiley: Weinheim, 2005; Chapter 14, pp 200−226.

(3) Willner, I. *Acc. Chem. Res.* **1997**, *30*, 347–356.

(4) Ziegler, C. in *Bioelectrochemistry*, Wilson, G. S., Ed.; Wiley-VCH: Weinheim, 2002; Chapter 2, pp 51−66.

(5) Willner, I.; Katz, E. in *Bioelectronics: From Theory to Applications*, Willner, I., Katz, E., Eds.; Wiley-VCH: Weinheim, 2005; Chapter 1, pp 1−13.

conjugated to redox centers. During the past years, a plethora of strategies involving different degrees of synthetic complexity were developed for redox-labeling diverse biomolecules with different purposes.[6]

Up to the present date, concanavalin A (Con A) remains the best studied among lectins. Its occurrence in high concentration in the jack bean (*Canavalia ensiformis*), ease of purification, and ability to bind mannose, which is widely distributed in naturally occurring glycoconjugates, account for the attention received by the lectin. Con A has been sequenced and its detailed three-dimensional structure worked out.[7] In addition to its use in the isolation and characterization of various glycoconjugates, Con A has been employed as a tool for a variety of studies. More recently, several investigators studied the usefulness of Con A as an effective ligand in the immobilization of glycoenzymes; Con A is a lectin protein found in jack bean and exists as a tetramer with a molecular mass of 104 kDa at a neutral pH.[7] Each Con A monomer contains one calcium ion binding site, one transition metal binding site, and one carbohydrate binding site (specific to α-D-mannose and α-D-glucose), also referred to as the combining site.[8,9] The strategy of incorporating predesigned redox centers into the Con A molecules could open up the possibility of facilitating or "wiring" the electron transfer between a glycoenzyme or other mannose/glucose-containing biomolecule and the electrode surface via a biosupramolecular assembly approach. Along these lines, we propose here an alternative biosupramolecular concept to create redox-active biobuilding blocks. Notably, in spite of the increasing interest in exploiting the biorecognition properties of Con A at electrochemical interfaces,[10−13] the incorporation of redox centers into the lectin periphery and its application to the construction of redox-active, stimuli-responsive biointerfaces has not been reported so far. These redox-labeled lectins could be considered as artificially generated bifunctional bioinorganic hybrids with the inorganic part being in charge of the redox mediation, and the protein itself provides the biomolecular recognition properties.

In this work, the labeling of Con A with a redox probe through a spacer is presented. The modified protein shows the same ability compared to the native one to recognize mannose-modified surfaces. Fluorescence and SAXS studies show that the conjugate presents slight changes in its conformation, whereas electrochemical results indicate that electron transfer across the bioconjugate-modified electrodes is feasible. Finally, we show the application of these redox-active biobuilding blocks to the construction of enzymatic electrodes through the recognition-directed assembly of glucose oxidase and electroactive Con A multilayers on mannose-modified Au electrodes.

Experimental Section

Materials. Concanavalin A (Con A—*Canavalia ensiformis* from jack bean), *N*-(3-dimethyl-aminopropyl)-*N*′-ethylcarbodiimide hydrochloride (EDC), *N*-hydroxysuccinimide (NHS), 8-(amino)octanoic acid (ω-aminocaprylic acid), bovine serum albumin (BSA), carbonic anhidrase II (CA, bovine erythrocytes), sinapinic acid (SA), cystamine dihydrochoride (Cys), α-D-mannopyranosylphenyl isothiocyanate (Man), and β-D-glucose were purchased from Sigma. Glucose oxidase (GOx, *Apergillus niger*) was obtained from Calzyme Laboratories, Inc. FMOC-PEG-COOH was provided by Novabiochem. The $[Os^{II}(bpy)_2ClpyCHO]$-PF_6 was synthesized as previously described[14] where bpy stands for bipyridine and pyCHO for pyridine-4-aldehyde. All other reagents were analytical grade.

Synthesis of $Os(bpy)_2ClpyCH_2$-8-(amino)octanoic Acid. Three milliliters of $[Os(bpy)_2ClpyCHO]PF_6$ (48 mg, 0.06 mmol) in methanol was added to a solution of 8-(amino)octanoic acid (11 mg, 0.07 mmol) and *p*-toluenesulfonic acid (2 mg 0.01 mmol) in methanol (2 mL). The mixture was left to react with stirring under argon atmosphere at 20 °C for 20 h. Afterward, the mixture was treated with an excess of sodium borohydride (6 mg, 0.16 mmol) and stirred overnight at room temperature. NaOH 1 M (2 mL) was added to quench the reaction, and the mixture was stirred for another 15 min and then extracted with CH_2Cl_2 (3 × 5 mL). The extract was washed with HCl 1 M saturated with NaCl (3 × 10 mL), dried ($MgSO_4$), and evaporated in vacuo. The dark brown solid was dissolved in 5 mL of CH_3CN and added to a large amount of ether (100 mL). The osmium derivative is not readily soluble in ether and precipitates as a fine brown solid. It is then filtered, washed with cold ether, and allowed to air-dry. Yield 32 mg (56%). ^{1}H NMR (200 MHz, dmso-d_6): δ for bpy-ring 8.52 (dd, 4H), 7.83 (m, 4H), 7.68 (dd, 4H), 7.24 (m, 4H); for py-ring 8.64 (dd, 2H), 7.92 (dd, 2H); for caprylic linker 4.46 (s, 2H), 2.78 (t, 2H), 2.09 (t, 2H), 1.92 (s, 1H), 1.56 (m, 4H), 1.24 (m, 6H). LD-MS: the signal at m/z = 791 and its isotopic distribution is consistent with $[Os(bpy)_2Clpy\text{-}C_8 + H]^+$ (spectrum is provided in the Supporting Information).

Synthesis of $Os(bpy)_2ClpyCH_2NH$-PEG-COOH. The procedure employed was analogous to that described early for the synthesis of $Os(bpy)_2ClpyCH_2$-8-(amino)octanoic acid. Previous to the conjugation reaction, the Fmoc group in the PEG derivative was removed by treating with piperidine 20% in DMF. Yield 35 mg (52%). ^{1}H NMR (200 MHz, dmso-d_6): δ for bpy-ring 8.52 (dd, 4H), 7.84 (m, 4H), 7.68 (dd, 4H), 7.26 (m, 4H); for py-ring 8.62 (dd, 2H), 7.92 (dd, 2H); for PEG linker 4.35 (s, 1H), 4.26 (s, 2H), 3.96 (s, 2H), 3.58 (s, 2H), 3.38 (s, 8H), 3.03−3.24 (m, 6H), 2.57 (t, 2H), 1.96 (s, 1H), 1.63 (m, 4H). LD-MS: the signal at m/z = 968 and its isotopic distribution is consistent with $[Os(bpy)_2Clpy\text{-}PEG + H]^+$ (spectrum is provided in the Supporting Information).

Synthesis of Osmium-Labeled Concanavalin A. The synthesis of Os-Con A derivatives was accomplished following a procedure described in the literature.[15,16] Briefly, Os-$(bpy)_2ClpyCH_2$-8-(amino)octanoic acid (16 mg, 0.02 mmol) or

(6) (a) Di Giusto, D. A.; Wlassoff, W. A.; Giesebrecht, S.; Gooding, J. J.; King, G. C. *Angew. Chem., Int. Ed.* **2004**, *43*, 2809–2812. (b) Radi, A.-E.; Sánchez, J. L. A.; Baldrich, E.; O'Sullivan, C. K. *J. Am. Chem. Soc.* **2006**, *128*, 117–124. (c) Willner, I.; Zayats, M. *Angew. Chem., Int. Ed.* **2007**, *46*, 6408–6418. (d) Baker, B. R.; Lai, R. Y.; Wood, M. S.; Heeger, A. J.; Plaxco, K. W. *J. Am. Chem. Soc.* **2006**, *128*, 3138–3139. (d) Azzaroni, O.; Álvarez, M.; Abou-Kandil, A. I.; Yameen, B.; Knoll, W. *Adv. Funct. Mater.* **2008**, *18*, 3487–3496. (e) Mir, M.; Álvarez, M.; Azzaroni, O.; Tiefenauer, L.; Knoll *Anal. Chem.* **2008**, *80*, 6564–6569. (f) Salmain, M. in *Bioorganometallics*, Jaouen, G., Ed.; VCH-Wiley: Weinheim, 2006; Chapter 6, pp 181−213.

(7) (a) Kantardjieff, K. A.; Höchtl, P.; Segelke, B. W.; Tao, F.-M.; Rupp, B. *Acta Crystallogr.* **2002**, *D58*, 735–743. (b) Deacon, A.; Gleichmann, T.; Kalb, A. J.; Price, H.; Raftery, J.; Bradbrook, G.; Yariv, J.; Helliwell, J. R. *J. Chem. Soc., Faraday Trans.* **1997**, *93*, 4305–4312. (c) Arrondo, J. L. R.; Young, N. M.; Mantsch, H. H. *Biochim. Biophys. Acta* **1988**, *952*, 261–268. (b) Edelman, G. M.; Cunningham, B. A.; Reeke, G. N., Jr.; Becker, J. W.; Waxdal, M. J.; Wang, J. L. *Proc. Natl. Acad. Sci. U.S.A.* **1972**, *69*, 2580–2584.

(8) (a) Hardman, K. D.; Agarwal, R. C.; Freiser, M. J. *J. Mol. Biol.* **1982**, *157*, 69–86. (b) Alter, G. M.; Pandolfino, E. R.; Christie, D. J.; Magnuson, J. A. *Biochemistry* **1977**, *16*, 4034–4038.

(9) (a) Becker, J. W.; Reeke, G. N., Jr.; Cunningham; Edelman, G. M. *Nature* **1976**, *259*, 406–409. (b) Kalb, A. J.; Levitzki, A. *Biochem. J.* **1968**, *109*, 669–672. (c) Derewenda, Z.; Yariv, J.; HelliwelI, J. R.; Kalb, A. J.; Dodson, E. J.; Papiz, M. Z.; Wan, T.; Campbell, J. *EMBO J.* **1989**, *8*, 2189–2193.

(10) Liu, S.; Wang, K.; Du, D.; Sun, Y.; He, L. *Biomacromolecules* **2007**, *8*, 2142–2148.

(11) (a) Dai, Z.; Kawde, A.-N.; Xiang, Y.; La Belle, J. T.; Gerlach, J.; Bhavanandan, V. P.; Joshi, L.; Wang, J. *J. Am. Chem. Soc.* **2006**, *128*, 10018–10019. (b) Ding, L.; Cheng, W.; Wang, X.; Ding, S.; Ju, H. *J. Am. Chem. Soc.* **2008**, *130*, 7224–7225.

(12) (a) Sato, K.; Kodama, D.; Anzai, J.-i. *Anal. Bioanal. Chem.* **2006**, *386*, 1899–1904. (d) Hoshi, T.; Akase, S.; Anzai, J.-i. *Langmuir* **2002**, *18*, 7024–7028.

(13) (a) Shen, Z.; Huang, M.; Xiao, C.; Zhang, Y.; Zeng, X.; Wang, P. G. *Anal. Chem.* **2007**, *79*, 2312–2319. (b) Guo, C.; Boullanger, P.; Jiang, L.; Liu, T. *Biosens. Bioelectron.* **2007**, *22*, 1830–1834.

(14) Danilowicz, C.; Cortón, E.; Battaglini, F. *J. Electroanal. Chem.* **1998**, *445*, 89–94.

(15) Soham, B.; Migron, Y.; Riklin, A.; Willner, I.; Tartakovsky, B. *Biosens. Bioelectron.* **1995**, *10*, 341–352.

$Os(bpy)_2ClpyCH_2NH$-PEG-COOH (20 mg, 0.02 mmol), NHS (15 mg, 0.13 mmol), and EDC (31 mg, 0.16 mmol) in 0.5 mL of dry DMF were heated with stirring at 80 °C under argon atmosphere for 1 h. After cooling the mixture to room temperature, portions of this solution were added to a 10 mg/mL Con A solution in phosphate buffer (0.1 M, pH 8.5). The mixture was left to react at room temperature overnight under smooth stirring. To remove unreacted osmium, the solution of modified Con A was purified using a series of two Hitrap desalting columns (GE Healthcare, 5 mL each) with phosphate buffer (25 mM, pH 7.4) at an elution rate of 3 mL/min. The product was then dialyzed at 4 °C for 24 h against Milli-Q water using a 3500 MWCO membrane and lyophilized. The Os/Con A ratio was determined by MALDI-TOF spectrometry.

Matrix-Assisted Laser Desorption-ionization Mass Spectrometry (MALDI-TOF-MS). MALDI-TOF mass spectra were recorded using an Omniflex Bruker Daltonics mass spectrometer operated in linear mode with the detector under positive polarity scan mode with a 1.650 V gain. Accelerating parameters were set to Ion source 1 (IS1), 19 kV; IS2, 15 kV; lens, 9.3 kV. Ionization was achieved by irradiation with a nitrogen laser (λ = 337 nm) operating at 5 Hz with 200 ns of pulsed ion extraction delay. The photomatrix solution was prepared by dissolving sinapinic acid to 1% in acetonitrile/0.1% TFA (70:30 v/v) solution. All samples and standards were prepared as 1 μM aqueous solution. A sandwich-like procedure was employed for spotting the samples. First, 0.3 μL of the photomatrix solution is spotted to the target plate and left to air-dry. Next, 0.3 μL of the protein solution is applied and allowed to air-dry, followed by the spotting of 0.3 μL of photomatrix solution. Prior to acquisition of spectra, excess matrix was removed with 15 shots at a laser power of 80%. Each spectrum is recorded for the mass range of 10 to 50 kDa with 50 shots at a fixed laser power of 65% and maximum laser frequency. The instrument was calibrated against BSA [$(M+H)^+$ = 66431 and $(M+2H)^{2+}$ = 33216] and CA [$(M+H)^+$ = 29025 and $(M+2H)^{2+}$ = 14513]. Bruker flexAnalysis software was used to calibrate the spectra by using the data collected from the BSA and CA spectra.

Construction of Self-Assembled Layers. The construction of molecular assemblies was prepared using a BK7 glass coated with 2 nm of chromium and 50 nm of gold by evaporation. The substrate was incubated overnight with a 5 mM ethanolic cystamine dihydrochoride solution. Afterward, the electrode was rinsed with ethanol and dried with N_2 followed by 2 h incubation in a 10 μg mL^{-1} α-D-mannopyranosylphenyl isothiocyanate solution in 0.05 M pH 7.4 PBS buffer. Then, the electrode was rinsed with PBS buffer and immersed for 1 h in a 1 μM Con A or Os-Con A solution in PBS buffer containing $CaCl_2$ 0.5 mM and $MnCl_2$ 0.5 mM. The same buffer was used to incorporate the GOx to the surface and to rinse the electrode after a Con A, Os-Con A, or GOx assembly step. To immobilize the enzyme onto the Os-Con A-modified surface, the electrode was incubated for 1 h in a 1 μM GOx solution. All steps were carried out at room temperature (ca. 20 °C).

Surface Plasmon Resonance (SPR) Spectroscopy. SPR detection was carried out in a homemade device using the Kretschmann configuration. The SPR substrates were BK7 glass slides evaporation-coated with 2 nm of chromium and 50 nm of gold. To estimate the biomolecule coverage during the sequential recognition-directed assembly steps, the SPR signal at different angles was recorded prior to and after injection of the corresponding protein solution in the liquid cell. This was done to detect the shift of the minimum angle of reflectance due to the protein assembly on the surface. The SPR angle shifts were converted into mass uptakes via the experimentally determined relationship, Γ (nanograms per square millimeter) = $\Delta\theta$ (degrees)/0.19. The sensitivity factor was obtained by procedures reported in the literature.[17,18]

Electrochemical Measurements. Cyclic voltammetry experiments were performed with a μAutolab potentiostat (Echo Chemie) using a three-electrode cell equipped with an Ag/AgCl (3 M KCl) reference electrode and platinum mesh counter electrode. All electrochemical experiments were carried out at room temperature (ca. 20 °C) in a Teflon cell designed in a way that exposes to solution a 0.18 cm^2 surface of the electrode. Electrochemical experiments were carried out in a 0.05 M KH_2PO_4/K_2HPO_4, 0.1 M KCl buffer solution, pH 7.4.

Small-Angle X-ray Scattering (SAXS) Characterization. SAXS experiments were performed using the D02B-SAXS1 beamline of the Laboratorio Nacional de Luz Sincrotron (Campinas, Brazil). The sample-to-detector distance was set to 415 mm and the working wavelength was 0.1488 nm. Sample temperature was kept to 22 °C using a circulating water bath. Two parallel micas were used as windows defining a 1 mm optical path sample chamber. The concentration of Concanavalin A in each experiment was 2 g L^{-1} in 0.05 M KH_2PO_4/K_2HPO_4, 0.1 M KCl buffer solution, pH 7.4. Each spectrum was corrected for beam attenuation and time integrated photon flux following normal procedures, and the corresponding buffer scattering was subtracted from each spectrum before analysis. The gyration radius R_g of the different Concanavalin A variants was obtained by analysis of SAXS patterns as Guinier plots ($\ln(I) = \ln(I_o) - R_G q^2/3$, $q = 4\pi \sin(\theta)/\lambda$, $qR_G \leq 1$). The globularity of each variant was assessed using the Kratky plot ($I(q) \times q^2$ vs q). The pair-distance distribution function (PDDF) was obtained using the regularized transform method proposed by Svergun et al. and implemented in the program *GNOM 4.51*.[19] Simulated SAXS plots were obtained using the program *CRYSOL 2.6*.[20]

Steady-State Fluorescence Studies and Light Scattering Experiments. Steady-state fluorescence experiments were performed using a Cary Eclipse spectrofluorimeter (Varian Inc. Australia). Tryptophan fluorescence emission was excited at 285 nm (5 nm entrance slit) and recorded in the range 305−405 nm (5 nm entrance slit). Protein concentration was 0.1 g L^{-1} in 0.05 M KH_2PO_4/K_2HPO_4, 0.1 M KCl buffer solution, pH 7.4. Light scattering experiments were performed using the same spectrofluorimeter recording the elastic light scattering at θ = 90° from the incident light beam.

Results and Discussion

Synthesis and Characterization of $[Os(bpy)_2Clpy]$-Modified Concanavalin A. First, we proceeded to the synthesis of the $[Os(bpy)_2Clpy]^+$ derivatives with the corresponding spacers bearing carboxylate terminal groups. This was accomplished by reacting 8-(amino)octanoic acid with $[Os(bpy)_2ClpyCHO]PF_6$ in methanol in the presence of *p*-toluenesulfonic acid. The different steps involved the ConA labeling with two different spacers (8-(amino)octanoic acid and H_2N-PEG-COOH) are depicted in Figure 1, and details are given in the Experimental Section. For the sake of simplicity, hereinafter we will refer to these compounds as $Os(bpy)_2Clpy$-PEG and $Os(bpy)_2Clpy$-C_8 linker, respectively (Figure 1). These probes bearing a carboxylate moiety are ready to react with the lysine residues present in Con A.

To measure the extent of the modification to the lysine residues with redox centers, the native Con A as well as their redox-tagged derivatives were analyzed by matrix-assisted laser desorption/

(16) Padeste, C.; Grubelnik, A.; Tiefenauer, L. *Biosens. Bioelectron.* **2003**, *19*, 239–244.
(17) Stenberg, E.; Persson, B.; Roos, H.; Urbaniczky, C. *J. Colloid Interface Sci.* **1991**, *143*, 513–526.
(18) Yu, F. Ph.D. Thesis, Johannes Gutenberg-Universität, Mainz, Germany, 2004; http://mpip-mainz.mpg.de/knoll/publications/thesis/yu_2004.pdf.
(19) Svergun, D. I. *J. Appl. Crystallogr.* **1992**, *25*, 495–503.
(20) Svergun, D. I.; Barberato, C.; Koch, M. J. H. *J. Appl. Crystallogr.* **1995**, *28*, 768–773.

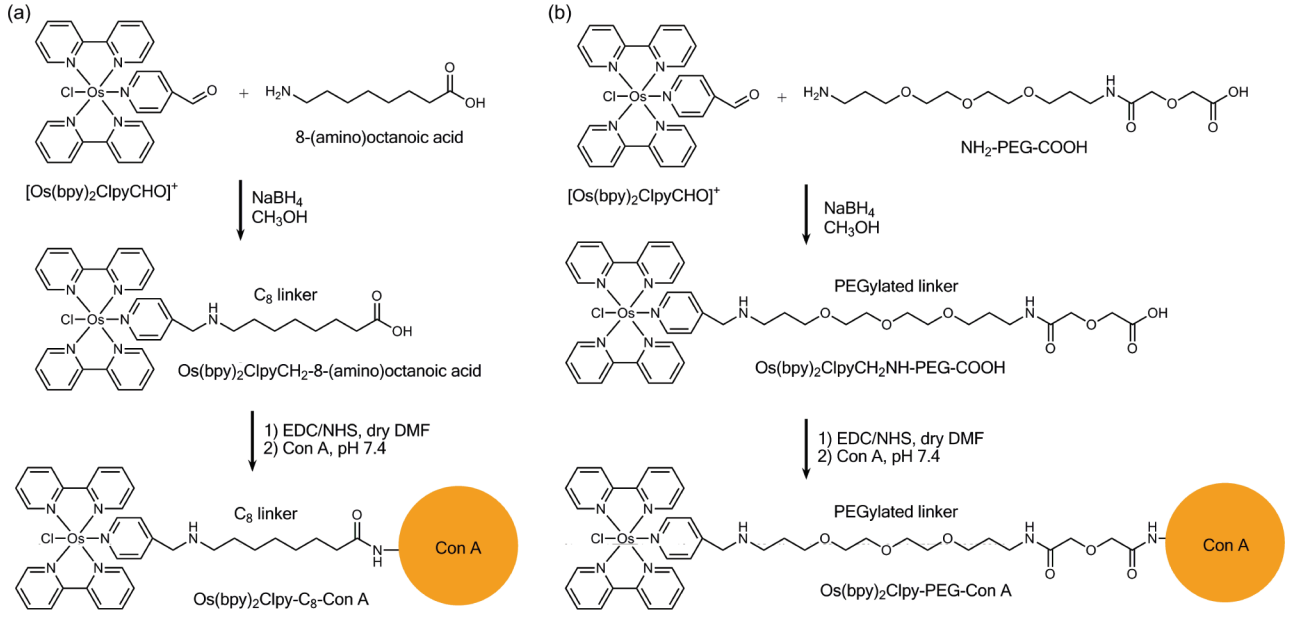

Figure 1. Reaction schemes describing the synthesis Os(II)-modified concanavalin A bearing aminooctanoic (a) and PEGylated (b) linkers.

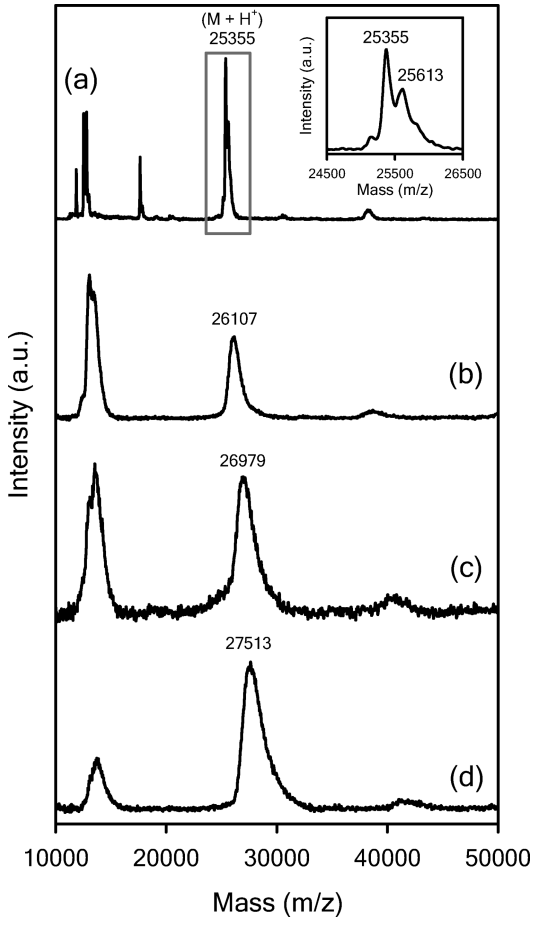

Figure 2. MALDI-TOF mass spectra of Con A with different degrees of modification: (a) native protein, (b) ([Os(bpy)$_2$Clpy]-C$_8$)$_4$-Con A, (c) ([Os(bpy)$_2$Clpy]-C$_8$)$_8$-Con A, (d) ([Os(bpy)$_2$Clpy]-C$_8$)$_{11}$-Con A.

ionization time-of-flight mass spectrometry (MALDI-TOF-MS) (Figure 2).

MALDI-TOF-MS can be used in several ways to provide a readout of the covalent modifications that occur upon reaction with a redox-active labels.[21] The simplest, but very useful, way is to monitor the average number of covalently bound linkers that modify the Con A structure. Comparing the mass spectrum of the native Con A prior to and after the reaction with the redox labels readily provides relevant information about the maximum number of labels and/or the average number of labels conjugated to the protein, i.e., the Os/Con A ratio .

Table 1. Degree of Derivatization and Molecular Mass of Different Redox-Active Con a Proteins, as Determined by MALDI-TOF-MS

linker	redox centers per Con A, *n*	molecular mass, Da (tetrameric form)
Native	0	101 420
Os(bpy)$_2$Clpy-C$_8$	4	104 428
Os(bpy)$_2$Clpy-C$_8$	8	107 916
Os(bpy)$_2$Clpy-C$_8$	11	110 052
Os(bpy)$_2$Clpy-PEG	12	113 624

Figure 2 shows the MALDI-TOF-MS spectra corresponding to Con A and its redox derivatives (MALDI-TOF mass spectra of ([Os(bpy)$_2$Clpy]-PEG)$_{12}$-Con A is described in the Supporting Information). Con A is a tetrameric protein in which the molecular mass of each monomer unit corresponds to 25 500 Da. Typically, a mass spectrum of the intact protein provides the precise molecular mass of the major and minor forms of the protein. In the case of native Con A, the signal detected at m/z = 25 355 corresponds to the mass-to-charge ratio of single-charged monomer units. A detailed view of this signal reveals the presence of a doublet, instead of a singlet, corresponding to m/z 25 355 and 25 613, respectively. This could be attributed to the presence of monomers with slightly different molecular masses owing to the presence of saccharides or metal ions (Ca^{2+} or Mn^{2+}) in the different monomer units. Large ions, like proteins and peptides, are typically multiply charged by added protons. Hence, the presence of doubly charged ions explains the appearance of signals in the 12 000 < m/z < 14 000 range.

MALDI-TOF mass spectra of Con A derivatized with different amounts of redox-active sites revealed the presence of signals at

(21) (a) Mann, M.; Hendrickson, R. C.; Pandey, A. *Annu. Rev. Biochem.* **2001**, *70*, 437–473. (b) Mendoza, L. V.; Vachet, R. W. *Mass Spectrom. Rev.* **2009**, *28*, 785–815.

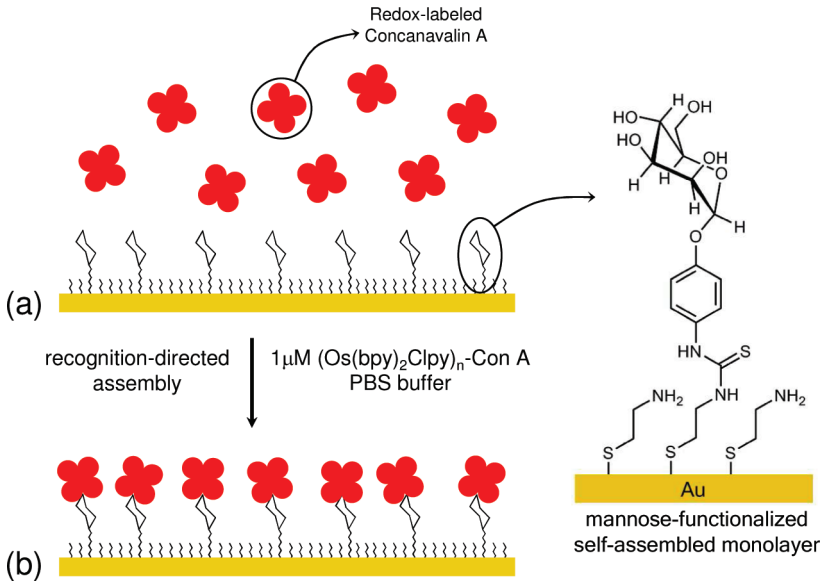

Figure 3. Scheme describing the functionalization of the gold electrodes with mannose groups (a) and the subsequent recognition-directed assembly of redox-active Con A (b).

higher $[M+H]^+$ values, thus indicating an increase in the molecular mass of the protein or, in other words, the successful covalent incorporation of the redox-labels into the protein structure. Formation of doubly charged ions was observed giving a separated second ion distribution at lower m/z values. The relative signal intensities of the doubly protonated species decrease with the molecular weight of the polymer when compared to the singly charged species. From this set of experimental results, and taking into account the molecular mass of the redox tags, we were able to determine the average number of redox labels incorporated into Con A (see Table 1).

Tagging was carried out under mild conditions to minimally compromise the protein structures and to ensure viable biomolecular recognition. The impact of Con A modifications on the carbohydrate−lectin interactions was assessed by surface plasmon resonance (SPR) spectroscopic experiments.[22] We studied the binding properties of the whole set of proteins in order to compare and gain an understanding of the impact of labeling on protein interactions with a view toward applications in recognition-directed assembly of functional biosupramolecular architectures. To achieve this goal, we estimated the maximum binding capacity defined as the maximum protein coverage obtained under saturation conditions. Recent surface plasmon resonance imaging studies by Corn and co-workers revealed that maximum coverage of native Con A on mannosylated surfaces is reached by incubating the samples under micromolar conditions.[23]

To perform these affinity assays, we modified gold films with mannose groups following the experimental protocol described by Willner and co-workers[24] for the immobilization of Con A via carbohydrate−lectin interactions (Figure 3). Gold-coated glass slides were treated with an ethanolic solution of cystamine. The resulting self-assembled cystamine monolayer-modified surface was then modified with isothiocyanatophenyl α-D-mannopyranoside in phosphate buffer (pH = 7.4), to yield the thiourea-monosaccharide monolayer-modified electrodes of phenyl α-D-mannopyranoside (Figure 3). Once the surfaces were functionalized, we

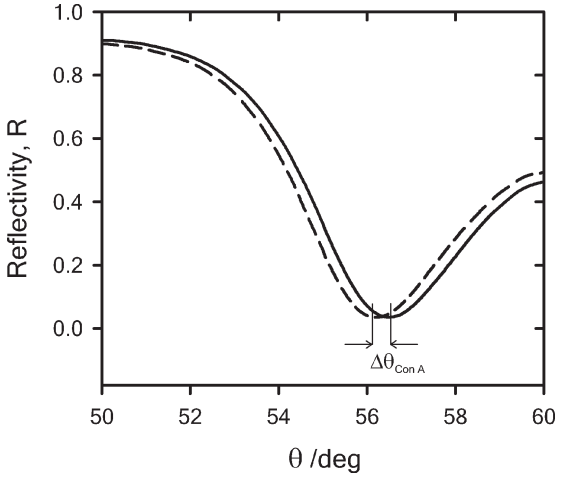

Figure 4. Reflected intensity as a function of the angle-of-incidence scan (θ) for a mannosylated Au electrode before (dashed line) and after (solid line) Con A binding (1 μM, pH 7.4). $\Delta\theta$ is proportional to the mass of native Con A immobilized on the electrode surface.

proceeded to monitor the formation of the glycoassemblies on the gold surfaces and estimate the mass coverages of the respective building blocks under saturation conditions, i.e., 1 μM Con A. In the case of native Con A, SPR measurements of the mannosylated gold surface prior to and after Con A assembly evidenced a well-defined shift in the minimum of the angular θ scans of reflected intensity (Figure 4). This $\Delta\theta$ is related to a mass uptake of 184 ng/cm^2 that corresponds to a surface coverage of 1.8 pmol/cm^2. This value is in good agreement with spectrophotometric measurements on Con A immobilized on quartz crystal by Anzai et al. who estimated 1.6 pmol/cm^2 for Con A monolayer coverage.[25] Analogous SPR experiments performed on redox-tagged Con A described a similar immobilization behavior leading to surface coverages comparable to those obtained for the native protein (SPR reflectivity curves are shown in the Supporting Information). Remarkably, proteins modified with 11 or 12 redox centers

(22) Knoll, W. *Annu. Rev. Phys. Chem.* **1998**, *49*, 569.
(23) Smith, E. A.; Thomas, W. D.; Kiessling, L. L.; Corn, R. M. *J. Am. Chem. Soc.* **2003**, *125*, 6140–6148.
(24) Willner, I.; Rubin, S.; Cohen, Y. *J. Am. Chem. Soc.* **1993**, *115*, 4937–4938.
(25) Anzai, J.-i.; Kobayashi, Y. *Langmuir* **2000**, *16*, 2851–2856.

Table 2. Mass Coverage of Different Redox-Active Con A Proteins, as Determined by Surface Plasmon Resonance (SPR) Studies

building block	mass coverage (ng/cm^2)	Γ (pmol/cm^2)
native Con A	184	1.81
(Os(bpy)$_2$Clpy-C$_8$)$_4$-Con A	198	1.89
(Os(bpy)$_2$Clpy-C$_8$)$_8$-Con A	205	1.90
(Os(bpy)$_2$Clpy-C$_8$)$_{11}$-Con A	202	1.84
(Os(bpy)$_2$Clpy-PEG)$_{12}$-Con A	208	1.83

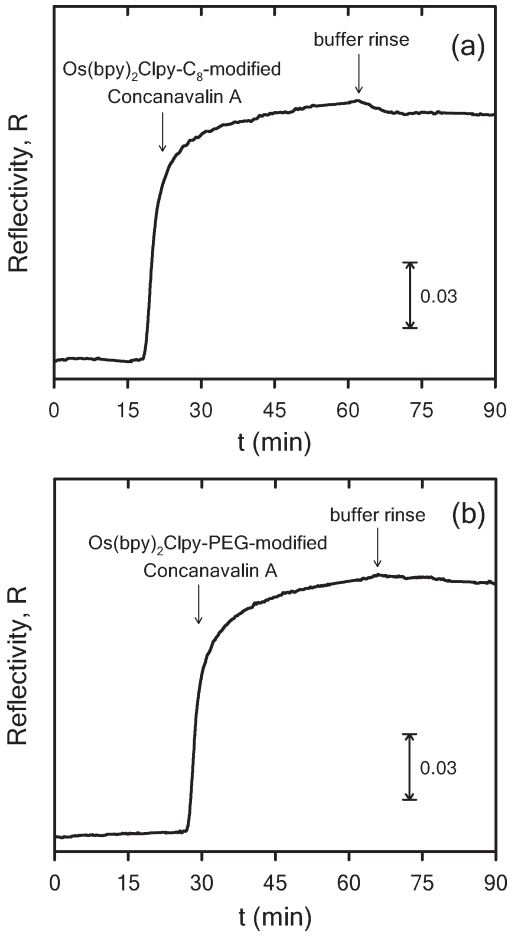

Figure 5. Time-resolved SPR sensorgram taken during the bioconjugation of (a) (Os(bpy)$_2$Clpy-C$_8$)$_{11}$-Con A and (b) (Os(bpy)$_2$-Clpy-PEG)$_{12}$-Con A. The kinetic scan describes the reflectivity changes after injection of 1 μM Os(II)-modified Con A into the liquid cell in contact with the mannosylated gold surface.

were able to attain surface coverages similar to the native unmodified protein (Table 2).

The interaction of (Os(bpy)$_2$Clpy-PEG)$_{12}$-Con A and (Os(bpy)$_2$Clpy-C$_8$)$_{11}$-Con A with the mannosylated surface was also examined by time-resolved SPR (Figure 5). Binding kinetics of heavily derivatized Con A displays the typical protein-specific profile arising from high affinity between ligand and receptor counterparts.[26] In close resemblance to previous results from Kahne et al. describing the recognition-mediated assembly of *Bauhinia purpurea* lectin on carbohydrate-modified self-assembled monolayers,[27] the mannosylated surfaces exhibited slow off-rates for the binding of the redox-modified Con A (see buffer rinse, Figure 5). In this regard, it is worth mentioning that slow dissociation rates represent a distinctive feature of multivalent interactions.[27,28] As such, these kinetic SPR measurements performed on (Os(bpy)$_2$Clpy-PEG)$_{12}$-Con A and (Os(bpy)$_2$Clpy-C$_8$)$_{11}$-Con A support the idea that polyvalent binding between the redox-tagged lectins and the sugar-modified surface occurs regardless of the extent of protein derivatization. These results corroborate that, in spite of the chemical modifications introduced in the protein periphery, its molecular recognition properties remain unaffected.

Steady-State Fluorescence Studies on Os(II)-Derivatized Concanavalin A. It is well-known that the intrinsic fluorescence emission spectra of proteins yield helpful information about the local environment of the emitting centers.[29] In particular, the quantum yield and the position of the maximum of tryptophan (Trp) fluorescence emission are solvent dependent, and hence, they can provide a complementary description of structural changes occurring in the protein. Each monomeric Con A contains four Trp at positions 40, 88,109, and 182, and seven tyrosines (Tyr) at 12, 22, 54, 67, 77, 100, and 176.[7] Even so, the fluorescence behavior of Con A is considered as that due to its Trp residues because the quantum efficiency of Tyr is much less than that of Trp in proteins.[30] The Trp moieties present in Con A absorbs appreciably at 280 nm giving a broad fluorescence with maximum at around 330−350 nm.

Figure 6a displays the different emission spectra obtained from Con A samples modified with increasing amounts of Os redox centers per protein (n). The decrease in the fluorescence intensity of the Trp residues (donor) with increasing acceptor concentration (n) clearly indicates that a quenching process is taking place in the hybrid bioinorganic building block. The modifications of the emission spectrum upon increasing the amount of redox centers covalently bound to the protein reflect that the microenvironments around the fluorophore in the protein solutions are quite different from that observed in the native Con A in the buffer solution. The decrease in fluorescence intensity can be ascribed to the strong quenching effect of Os(bpy)$_2$Clpy-X moieties on Trp fluorescence (Figure 6b). This strong effect is manifested even in the presence of small amounts of Os centers per molecule, i.e., $n = 4$. Pelley and Horowitz have shown from fluorescence quenching studies of Con A by iodide ions that two Trp residues are near the molecular surface.[31] Similarly, analysis of three-dimensional crystal structure data of Con A indicates that, out of the four Trps, only two (at 88 and 182) are on the molecular surface. In view of these results, the strong quenching effects evidenced in our experiments can be interpreted by considering that in Con A the outermost tryptophan residues are in close proximity to peripheral lysine residues (Figure 6b, inset), which participate in the covalent binding of the redox centers. The incorporation of Os centers has an immediate effect on the fluorescence of the more exposed sensitive Trp residues. Then, gradual incorporation of Os sites (increase in n) promotes further decrease in the fluorescence intensity of the Trp residues present in Con A.

Small-Angle X-ray Scattering (SAXS) Characterization of Concanavalin A and Its Os(II)-Derivatized Conjugates. To obtain detailed information about the structural characteristics of Con A and their redox-modified derivatives or elucidate the possible formation of aggregates in solution, our MALDI measurements were supplemented by SAXS studies.[32] Due to the

(26) Mann, D. A.; Kanai, M.; Maly, D. J.; Kiessling, L. L. *J. Am. Chem. Soc.* **1998**, *120*, 10575–10582.
(27) Horan, N.; Yan, L.; Isobe, H.; Whitesides, G. M.; Kahne, D. *Proc. Natl. Acad. Sci. U.S.A.* **1999**, *96*, 11782–11786.
(28) Kiessling, L. L.; Gestwicki, J. E.; Strong, L. E. *Angew. Chem., Int. Ed.* **2006**, *45*, 2348–2368.
(29) Lakowicz, J. R. *Principles of Fluorescence Spectroscopy*;Plenum Press: New York, 1983.
(30) Rao, M. V. R.; Atryi, M.; Rajeswari, M. R. *J. Biosci.* **984**, *6*, 823–828.
(31) Pelley, R.; Howorwitz, P. *Biochim. Biophys. Acta* **1976**, *427*, 359–363.

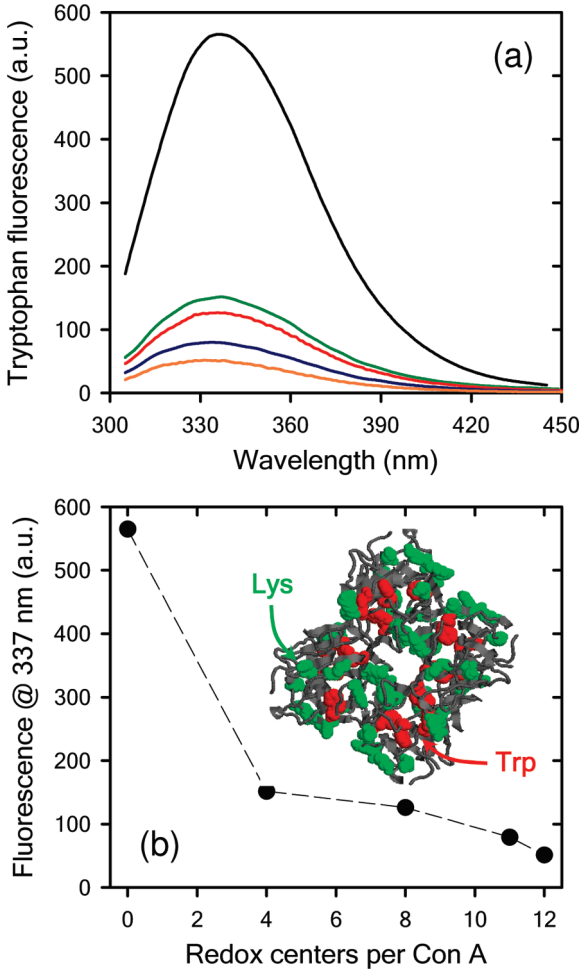

Figure 6. (a) Emission spectra corresponding to the following set of proteins: native Con A (black trace), $(Os(bpy)_2Clpy\text{-}C_8)_4$-Con A (green trace), $(Os(bpy)_2Clpy\text{-}C_8)_8$-Con A (red trace), $(Os(bpy)_2Clpy\text{-}C_8)_{11}$-Con A (blue trace), and $(Os(bpy)_2Clpy\text{-}PEG)_{12}$-Con A (orange trace). (b) Tryptophan fluorescence as a function of the number of $[(Os(bpy)_2Clpy]^+$ centers per Con A molecule. The error bars are smaller than the symbol size. Inset: Tetrameric native concanavalin A. For the sake of clarity, tryptophan and lysine residues were colored in red and green, respectively. The molecular image was generated from crystallographic data (RCSB Protein Data Bank 1BXH) using the *RasMol* molecular visualization program.

scarce information in the literature about SAXS characterization of Con A from jack bean, we will first introduce the scattering studies performed on native Con A in buffer solution (PBS, pH 7.4). Then, we will proceed to describe the SAXS experiments performed on the proteins modified with varying amounts of Os centers.

Figure 7a shows the scattering patterns obtained for 1 μM Con A solutions (0.1 M PBS buffer, pH 7.4). $I(q)$ is the scattered intensity at momentum transfer $q = (4\pi/\lambda) \sin \theta$, where λ is the wavelength of the radiation and 2θ is the scattering angle. The Kratky representation of the SAXS data has been used to analyze the globularity of the protein in solution (Figure 7b).[32] The Kratky plot of Con A in buffer solution at pH 7.4 shows a bell-shaped curve in agreement with the expected globular structure of the protein.

Relevant information about the shape of the biomacromolecules, as well as on the formation of aggregates, can be obtained by using the pair distance distribution function $P(r)$ (Figure 7c).[33] The corresponding $P(r)$ function was obtained by means of the regularization technique implemented in *GNOM 4.5*.[19] At pH 7.4, Con A is a tetramer with four identical subunits of molecular mass ~25.5 kDa each. X-ray crystallographic studies have established that the tetramer has extensive β-structure, approximately 60% overall. However, below pH 6.0, the tetramers dissociate into dimers as a result of the protonation of the imidazole groups of His-127 and His-51, which are located at the dimer/dimer interface. Structural studies indicated that the two dimers show a slight twist in the tetramer which aids in the overall packing.[7] In this context, the supramolecular structure of tetrameric Con A in solution (at pH 7.4) can be described as ellipsoidal dimers interacting primarily through side chains projecting from the large β-structure in the back of the molecule into the region of dimer−dimer contact.[7] It is worthwhile mentioning that the experimentally obtained $P(r)$ also resembles the pair distance distribution function derived form crystallographic data. Figure 7c shows the $P(r)$ function corresponding to the SAXS pattern obtained from native Con A in PBS buffer together with that simulated from the crystal structure of Con A (Protein Data Bank 1BXH). The differences between both curves are more pronounced around 6 nm, the region of the $P(r)$ dominated by the larger monomer-to-monomer distance within the tetrameric structure. In this regard, a reduction on the curve around 6 nm in the simulated data should not be surprising provided that strain due to packing forces in the crystallized protein may lead to reduction of the monomer-to-monomer distance.[34]

The linearity of the $\ln(I(q))$ vs q^2 plot also enables an accurate estimation of the radius of gyration, R_G, by means of the Guinier relation for the low q scattered intensity

$$I(q) = I(0) \exp\left(-\frac{q^2 {R_G}^2}{3}\right) \quad (1)$$

$I(0)$ is the extrapolation value of scattered intensity at $q = 0$. R_G can be extracted from the limiting slope at $q \rightarrow 0$ in the plots of the logarithm of $I(q)$ vs q^2 shown in Figure 7d . Table 3 lists all the geometrical values.

The radius of gyration of the native protein is compatible with that corresponding to a compact protein of ~102 kDa, which is the molecular mass of Con A. However, note that the radii of gyration of the derivatized proteins are significantly higher than that estimated for the native protein. A careful look to this information indicates that the size of the building blocks seems to be more dependent on the nature of the linker than on the degree of derivatization. This could be attributed to the hydrophobic nature of the aminooctanoic linker that affects the colloidal stability of derivatized protein. Conversely, as is well-known, PEGylated building blocks are commonly used to confer hydrophilic environments to biomolecules, thus inhibiting the formation of aggregates and flocculation.[35]

(32) (a) Vachette, P.; Svergun, D. in *Structure and Dynamics of Biomolecules: Neutron and Synchrotron Radiation for Condensed Matter Studies*, Fanchon, E.; Geissler, E.; Hodeau, J. L.; Regnard, J. R.; Timmins., P. A., Eds.; Oxford University Press: Oxford, 2000; Chapter 11.(b) Glatter, O.; Kratky, O. *Small-Angle X-Ray Scattering*; Academic Press: New York, 1982.

(33) (a) Rescic, J..; Vlachy, V.; Jamnik, A.; Glatter, O. *J. Colloid Interface Sci.* **2001**, *239*, 49–57. (b) Mittelbach, R.; Glatter, O. *J. Appl. Crystallogr.* **1998**, *31*, 600–608.

(34) (a) Leggio, C.; Galantini, L; Pavel, N. V. *Phys. Chem. Chem. Phys.* **2008**, *10*, 6741–6750. (b) Svergun, D. I.; Petoukhov, M. V.; Koch, M. H. J.; König, S. *J. Biol. Chem.* **2000**, *275*, 297–302. (c) Putnam, C. D.; Hammel, M.; Hura, G. L.; Tainer, J. A. *Q. Rev. Biophys.* **2007**, *40*, 191–285.

(35) Bailon, P.; Berthold, W. *Pharm. Sci. Tech. Today* **1998**, *1*, 352–356.

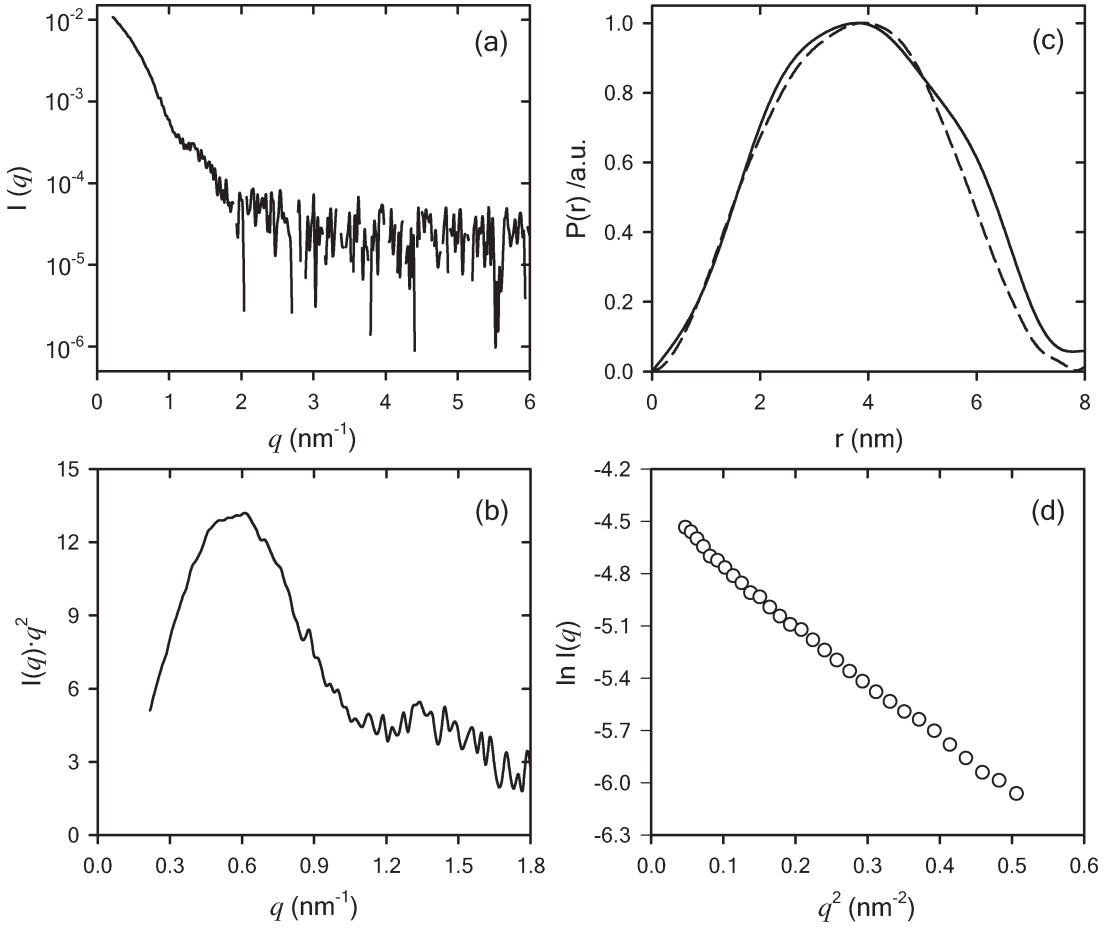

Figure 7. (a) Raw SAXS data corresponding to native Con A (1 μM in buffered solution, pH 7.4). (b) Kratky plot of data depicted in (a). Pair−distance distribution function, $P(r)$, obtained from data in (a) using the program *GNOM 4.5*. The dotted line corresponds to the $P(r)$ function obtained from the crystallographic data of Con A (RCSB Protein Data Bank 1BXH). (d) Guinier plot of the logarithm of the scattered intensity versus the squared momentum transfer for 1 μM native Con A in PBS buffer (pH 7.4).

Table 3. Radii of Gyration (R_G) Corresponding to Native Con A and Its Os(II)-Derivatized Conjugates, as Determined by Small-Angle X-ray Scattering (SAXS) Studies

building block	radius of gyration (nm)
Con A	2.86
$([Os(bpy)_2Clpy]^+$-$C_8)_4$-Con A	4.28
$([Os(bpy)_2Clpy]^+$-$C_8)_8$-Con A	4.15
$([Os(bpy)_2Clpy]^+$-$C_8)_{11}$-Con A	4.24
$([Os(bpy)_2Clpy]^+$-$PEG)_{12}$-Con A	3.80

Figure 8 describes the $P(r)$ for the redox-tagged proteins obtained from SAXS experiments in solution. It can be clearly seen that they differ from that obtained for the native Con A.

A large broadening of the pair-distance distribution function is observed, suggesting a morphological transition in which the scattering particles evolve from a globular-like structure (native Con A) to a more ellipsoidal-like structure. As described by Glatter et al., these transformations observed in the $P(r)$ are typical of the aggregation process, thus corroborating that the increasing R_G's are not due to the increasing size of the biohybrid building block itself but due to the presence of some aggregation in solution.[36] Note, however, that r_{max} obtained for $([Os(bpy)_2Clpy]^+$-$PEG)_{12}$-Con A coincides with that observed in the native protein. Furthermore, even though the $P(r)$ presents the typical elongation/extension observed in aggregated systems, the magnitude of this extension is more restricted than that observed in Con A proteins modified with aminooctanoic linkers. In agreement with the information derived from the R_G values, the $P(r)$ is indicating that $([Os(bpy)_2Clpy]^+$-$PEG)_{12}$-Con A in buffer solution is less aggregated than analogous systems constituted of $([Os(bpy)_2Clpy]^+$-$C_8)_n$-Con A.

With the aim of gathering complementary information on the extent of aggregation, we performed elastic scattering experiments of the fluorescence excitation light. The Rayleigh scattering theory predicts that light scattered by a particle varies as the square of the particle volume.[37] So, for an aggregation process where the total number of particles remains constant, the total amount of light scattered should increase in proportion to the average aggregate volume.

Figure 9 shows the variations in the normalized scattered light for the different redox-tagged proteins. From these experiments, we can conclude that proteins modified with caprilic linkers display a scattering behavior congruent with the formation of dimer and trimers in solution. In contrast, proteins modified with PEGylated linkers showed no evidence of significant aggregation. In this regard, we should mention that control experiments performed on Con A subjected to the same coupling conditions used to conjugate the redox centers revealed no significant differences

(36) Lehner, D.; Worning, P.; Fritz, G.; Øgendal, L.; Bauer, R.; Glatter, O. *J. Colloid Interface Sci.* **1999**, *213*, 445–456.

(37) Hiemenz, P. C.; Rajagopalan *Principles of Colloid and Surface Chemistry*; Marcel Dekker: New York, 1997; Chapter 5, pp 193−246.

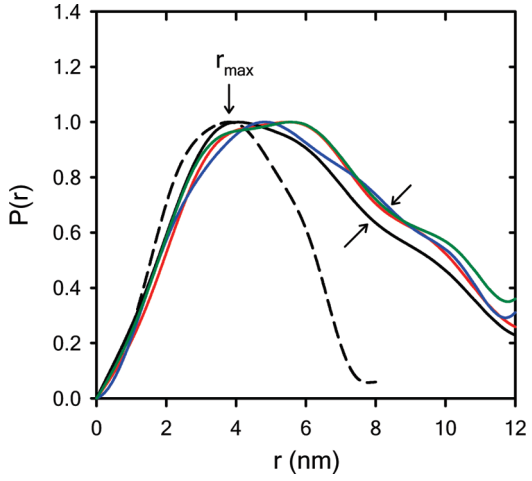

Figure 8. Pair−distance distribution function, $P(r)$, obtained from SAXS data using the program *GNOM 4.5*. The different traces correspond to (red trace) $(Os(bpy)_2Clpy\text{-}C_8)_4$-Con A, (green trace) $(Os(bpy)_2Clpy\text{-}C_8)_8$-Con A, (blue trace) $(Os(bpy)_2Clpy\text{-}C_8)_{11}$-Con A, and (black trace) $(Os(bpy)_2Clpy\text{-}PEG)_{12}$-Con A. For the sake of comparison, we have included the $P(r)$ function for the native Con A (dashed trace). The arrows indicate the broadening of $P(r)$ in the case of Con A proteins modified with aminooctanoic linkers.

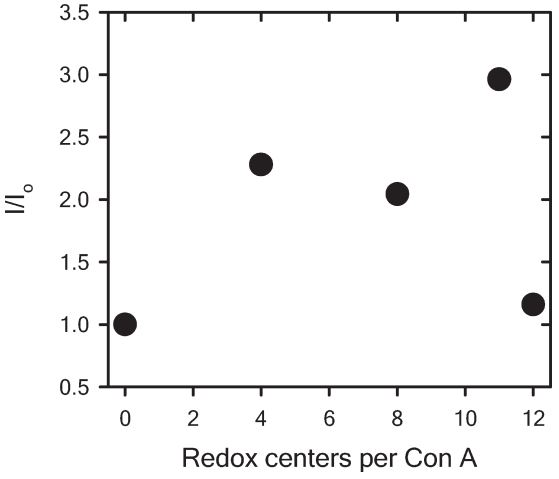

Figure 9. Representation of the scattered light (I) normalized to the signal obtained from the light scattering of native Con A (I_o) for different Os(II)-derivatized conjugates as a function of the degree of derivatizacion of the protein. The experiments were performed at room temperature. Protein concentration: 1 μM in PBS buffer, pH 7.4. The error bars are smaller that the symbol size.

in the lectin characteristics (see Supporting Information for details). Hence, we may conclude that the reaction environment provided solely by EDC + NHS does not promote cross-linking of the protein and the protein aggregation originates from the chemical characteristics of the linker.

These results univocally reinforce the idea that the chemical nature of the linkers plays a key role in determining the stability and aggregation properties of the biohybrid building blocks. Proteins derivatized at a similar extent may present remarkably different aggregation behavior depending on the functionalization via aminooctanoic or PEGylated bridges. The explanation of this contrasting behavior lies in the fact that oligoethylene groups are capable of organizing water into a near-protein phase with greatly increased viscosity, thus forming a physical barrier to inhibit protein−protein contacts. Steric hydration forces, such as this, have previously been invoked to explain the short-range (2−3 nm) repulsions seen for hydrophilic colloidal particles of silica and mica, as well as surfaces coated with cationic surfactants.[38] It has been demonstrated that a hydrophilic surrounding alone is not sufficient to produce the viscous interphase and that the presence of the ethylene glycol moieties are the principal factor that produces a unique repulsive behavior in the presence of water which, in turn, kinetically inhibits the approach of other "fouling" neighboring redox-tagged proteins.[38]

Electrochemical Characterization. For the electrochemical characterization, the redox-tagged proteins were supramolecularly assembled on mannosylated gold electrodes. Cyclic voltammograms of electrode-confined redox-derivatized Con A show the oxidation and reduction peaks corresponding to the $[Os(bpy)_2Clpy]^+$ moieties in the 0.25−0.35 V (vs Ag/AgCl) potential region, which is good agreement with previously reported formal potentials of similar redox centers (Figure 10a,b).[14]

As expected, the magnitude of the electrochemical response is proportional to the average number of Os centers incorporated on each Con A molecule (n). This linear correlation is also observed when the electrochemical charge (Q) is plotted against n (Figure 10c). At first sight, no significant changes between the overall voltammetric characteristics of $Os(bpy)_2Clpy^+\text{-}C_8$-Con A and $Os(bpy)_2Clpy^+$-PEG-Con A are observed. In a similar way, voltammetric data revealed that increasing the potential scan rate promotes neither substantial peak splitting nor significant drop of the voltammetric charge, thus reflecting that the population of redox centers "connected" to the gold surface has no major kinetic limitations to charge transfer at the bioconjugate−electrode interface (voltammograms are provided in the Supporting Information).

If we consider the critical role played by redox connectivity in the overall electron transfer process, then one fundamental question emerges: What is the fraction of redox centers that are actually connected to the electrode? To answer this question, we compared the "entire population" of redox centers, as determined by SPR, with the "electroactive" population of redox centers, as determined by cyclic voltammetry.

These values are compiled in Table 4. It is evident from these data that an important fraction of the redox active sites are not actually connected to the gold surface. This implies that the architecture of the interfacial bioassembly has an important effect on the electron transfer characteristics of the redox conjugate. From comparing and contrasting information derived from cyclic voltammetry at high scan rates, we can infer that, while a major fraction of redox centers remain electrochemically inactive, the active ones are able to participate in the electron transport without significant hindrance. Another interesting aspect of the data listed in Table 4 is the fact that, independently of the actual number of redox sites, proteins modified with 8, 11, or 12 $Os(bpy)_2Clpy^+$ moieties display the same fraction of electroactive sites, i.e., 0.3, while in proteins bearing 4 redox centers, the electroactive fraction is only 0.2. The n-dependent variation in the electroactive fraction of redox centers may suggest the presence of percolation effects. In other words, a critical density of redox sites should be reached in order to optimize the electronic connectivity within the electroactive assembly. The charge percolation should take place by hopping between adjacent $Os(bpy)_2Clpy^+$ centers within the protein film. To check this hypothesis, we investigated in more detail the influence of n on the electrochemical charge (Q) determined by cyclic voltammmetry. Figure 10d shows Q

(38) Kim, H. I.; Kushmerick, G.; Houston, J. E.; Bunker, B. C. *Langmuir* **2003**, *19*, 9271–9275.

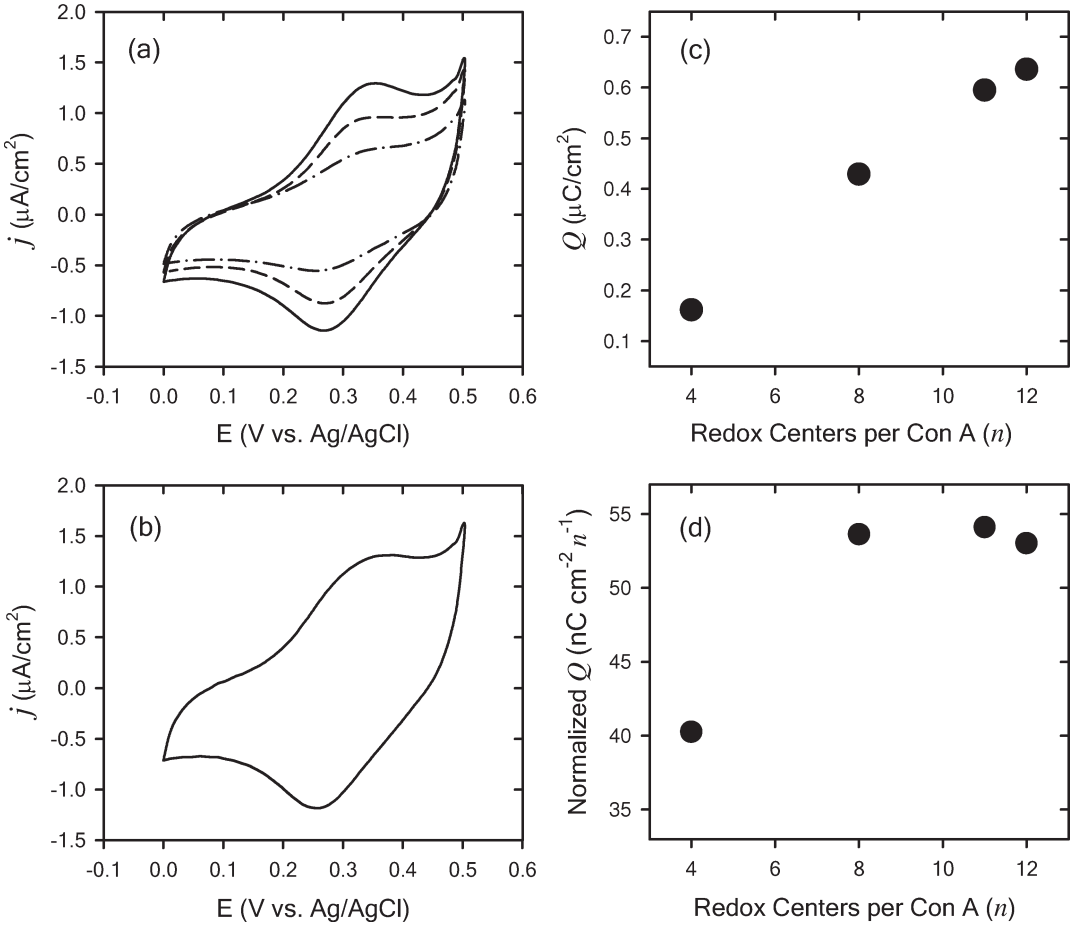

Figure 10. (a) Cyclic voltammograms of Os(II)-derivatized Con A immobilized on gold electrodes corresponding to $(Os(bpy)_2Clpy\text{-}C_8)_4$-Con A (dashed-dotted trace), $(Os(bpy)_2Clpy\text{-}C_8)_8$-Con A (dashed trace), and $(Os(bpy)_2Clpy\text{-}C_8)_{11}$-Con A (solid trace). T = 298 K, v = 100 mV/s. Electrolyte: 0.05 M KH_2PO_4/K_2HPO_4, 0.1 M KCl buffer solution, pH 7.4. (b) Cyclic voltammogram of $(Os(bpy)_2Clpy\text{-}PEG)_{12}$-Con A assembled on gold electrodes. T = 298 K. v = 100 mV/s. Electrolyte: 0.05 M KH_2PO_4/K_2HPO_4, 0.1 M KCl buffer solution, pH 7.4. (c) Voltammetric charge of different Os(II)-derivatized Con A assemblies as a function of the number of redox centers per protein. (d) Voltammetric charge of redox-active Con A assemblies normalized to the number of redox moieties per protein a function of the degree of derivatization (n). The errors bars are smaller than the symbol size.

Table 4. Electroactive Population and Total Population of Redox Centers for the Different Os(II)-Derivatized Con A Conjugates, as Determined by Surface Plasmon Resonsnce Spectroscopy (SPR) and Cyclic Voltammetry (CV), Respectively

redox-active architecture	electroactive population (pmol/cm^2)	total population (pmol/cm^2)	electroactive fraction
$[Os(bpy)_2Clpy]^+\text{-}C_8)_4$-Con A	1.7	7.6	0.21
$[Os(bpy)_2Clpy]^+\text{-}C_8)_8$-Con A	4.5	15.2	0.30
$[Os(bpy)_2Clpy]^+\text{-}C_8)_{11}$-Con A	6.2	20.2	0.30
$[Os(bpy)_2Clpy]^+\text{-PEG})_{12}$-Con A	6.6	22	0.30

normalized to n, plotted against n. This representation provides a simple and quantitative idea of the average charge contribution of each electroactive moiety in the different redox-tagged proteins. This analysis is self-consistent provided that the information is derived from the same set of electrochemical experiments and SPR demonstrated that the surface coverages for the different assemblies are comparable. The plot describes a trend similar to the one shown in Table 4. In $([Os(bpy)_2Clpy]^+\text{-}C_8)_4$-Con A assemblies, the "nominal" average charge contribution per redox site is 40 nC/cm^2, whereas in $([Os(bpy)_2Clpy]^+\text{-}C_8)_8$-Con A, $([Os(bpy)_2Clpy]^+\text{-}C_8)_{11}$-Con A, and $([Os(bpy)_2Clpy]^+\text{-PEG})_{12}$-Con A assemblies, this contribution is 53 nC/cm^2. This implies that increasing the number of redox sites per protein from 4 to 8 leads to a 32% increase in redox connectivity. The overall voltammetric experiments indicate that the electron transfer across the redox-tagged protein film is feasible. In other words, despite the fact that the interface is constituted of a densely packed protein conjugate, a fraction of the confined $Os(bpy)_2Clpy^+$ moieties are "wired" to the gold electrode. In this regard, it worth indicating that a position-dependent role of the Os centers might be another possibility to explain the n-dependent variation in the electroactive fraction of redox centers. The higher double layer capacitance observed upon oxidation, as shown on the right of the voltammograms in Figure 10, can be attributed to a pronounced increase of surface charge in the $Os(bpy)_2Clpy^+$-Con A films. The double layer capacitance of molecular organic films has been extensively studied within theoretical and experimental frameworks.[39] This characteristic feature of the voltammetric response gives an indication of and provides information about the electrostatic state of the film. In general terms, the generation of charges into the surface layer leads to an increase of the double-layer capacitance. Upon oxidation, n positive charge units are electrochemically generated on each protein.[40] This means that to

(39) (a) Smith, C. P.; White, H. S. *Langmuir* **1993**, *9*, 1–3. (b) Bryant, M. A.; Crooks, R. M. *Langmuir* **1993**, *9*, 385–387.

every single bioconjugate molecule positive charges will be added by oxidizing the attached $Os(bpy)_2Clpy^+$ moieties, observed as an increased capacitance.

In this context, pulse voltammetric techniques were used in order to substantially increase the ratio between faradaic and nonfaradaic currents and, hence, obtain relevant information masked in the voltammetric data. In differential pulse voltammetry (DPV), fixed-magnitude pulses superimposed on a linear potential ramp are applied to the working electrode.[41] After the potential is stepped, the charging current decays rapidly (exponentially) to negligible values, whereas the faradaic current decays more slowly. Figure 11a shows the differential pulse polarograms obtained from $[Os(bpy)_2Clpy]^+$-$(C_8)_n$-Con A assemblies conjugated on mannosylated electrodes. As expected, DPV is a very sensitive technique and the increasing amounts of surface-confined $[Os(bpy)_2Clpy]^+$ centers in the different protein assemblies are easily detected in a very straightforward manner (Figure 11a). In addition, it is also observed that the density of attached redox centers per protein has no effect on the peak potential (E_p). The well-defined E_p obtained by DPV is often used for analytical purposes to identify species; however, in our case, we used this parameter to elucidate the influence of the linker on the formal potential of the redox centers, provided that

$$E_p = E_{1/2} - \Delta E/2 \quad (2)$$

where $E_{1/2}$ is the half-wave potential and ΔE is the pulse amplitude. Hence, comparison of DPV traces of different redox-tagged proteins obtained under similar pulse amplitude conditions leads to

$$\Delta E_p = \Delta E_{1/2} \sim \Delta E^\circ \quad (3)$$

ΔE° refers to the variation in formal potential of the redox centers (E°) as determined by DPV.

Figure 11b describes the DPV polarograms corresponding to $[Os(bpy)_2Clpy]^+$-$(C_8)_{11}$-Con A and $[Os(bpy)_2Clpy]^+$-$(PEG)_{12}$-Con A assemblies displaying E_p's of 0.29 and 0.26 V, respectively. It is evident that the presence of the PEGylated linker promotes a cathodic shift in the formal potential of the $[Os(bpy)_2Clpy]^+$.

In our experimental scenario, the purpose of explaining this difference in the formal potential of the $[Os(bpy)_2Clpy]^+$ lies in the fact that redox centers are very sensitive to the characteristics of the surroundings.[42] As is well-known, the thermodynamic characteristics of electroactive sites are strongly affected by the nature of the environment where they are placed.[43] Due to its thermodynamic origin, the magnitude of their formal potential can act as a reporter of subtle alterations in the physicochemical characteristics of their surroundings. In a seminal work, Rowe and Creager investigated the behavior of ferrocene moieties embedded in alkanethiolate SAMs of varying chain length.[44] They found that the formal potential for ferrocene oxidation was shifted to more positive values as the ferrocene group was buried deeper into the hydrophobic environment. This potential shift reached nearly 0.3 V when the scenario changed from ferrocene groups totally exposed to the electrolyte solution to the same electroactive

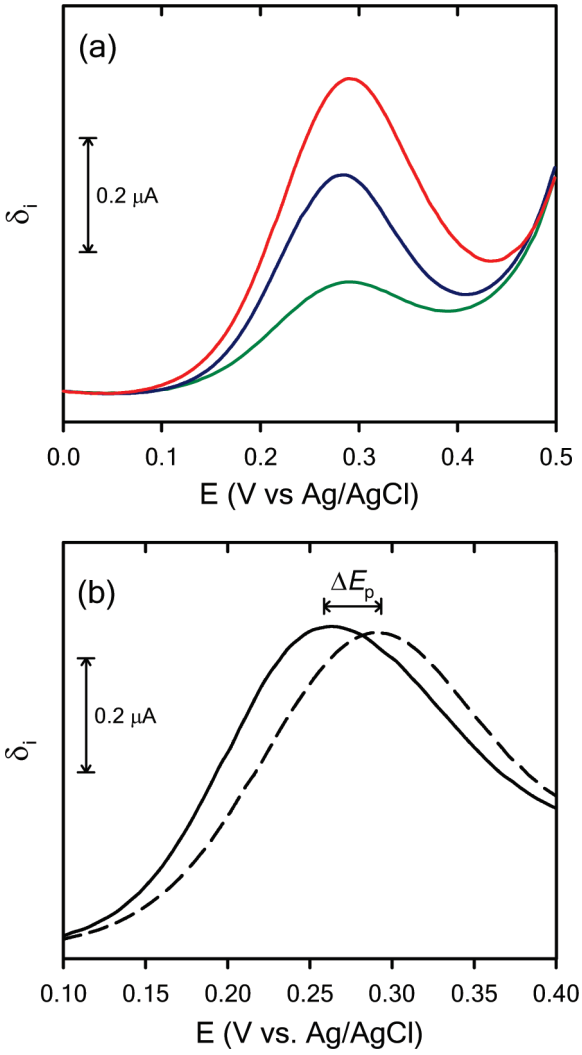

Figure 11. (a) Differential pulse voltammograms (DPV) describing the electroactive characteristics of $(Os(bpy)_2Clpy\text{-}C_8)_n$-Con A assemblies for $n = 4$ (green trace), 8 (blue trace), and 11 (red trace). (b) Comparative DPV analysis of $(Os(bpy)_2Clpy\text{-}C_8)_{11}$-Con A (dotted trace) and $(Os(bpy)_2Clpy\text{-}PEG)_{12}$-Con A (solid trace) illustrating the variation in E_p arising from the nature of linker. Parameters employed: pulse time (τ) 0.056 s; waiting period (τ') 0.5 s; initial potential 0 V; final potential 0.5 V; potential staircase 0.00495 V; pulse height (ΔE) 0.0495 V. Electrolyte: 0.05 M KH_2PO_4/K_2HPO_4, 0.1 M KCl buffer solution, pH 7.4.

groups surrounded by a long-chain alkanethiol. The characteristics of the local environment at the molecular level play a key role in determining the relative stability of species involved in the redox couple. In the latter case, electrogeneration of ferricenium species in a hydrophobic poorly solvated environment is energetically more costly than in exposed hydrophilic surroundings. This is experimentally reflected in a positive shift of the formal potential. In close resemblance to the ferrocene example, the PEG and aminooctanoic linkers introduce different solvation environments which, in turn, have an impact on the stability of the redox couples. In our case, the redox reaction of the $[Os(bpy)_2Clpy]^+$ labels involves the generation of $[Os(bpy)_2Clpy]^{2+}$species in the environment provided by the Con A. In this context, we hypothesize that the presence of a more hydrated environment in the presence of the PEG linker further stabilizes the generation of the divalent $[Os(bpy)_2Clpy]^{2+}$species, thus promoting a cathodic shift in the formal potential.

(40) Azzaroni, O.; Mir, M.; Álvarez, M.; Tiefenauer, L.; Knoll, W. *Langmuir* **2008**, *24*, 2878–2883.
(41) Wang, J. *Analytical Electrochemistry*; Wiley-VCH: New York, 2000; Chapter 3, p 68.
(42) (a) Madhiri, N.; Finklea, H. O. *Langmuir* **2006**, *22*, 10643–10651. (b) Haddox, R. M.; Finklea, H. O. *J. Phys. Chem. B* **2004**, *108*, 1694–1700.
(43) Azzaroni, O.; Yameen, B.; Knoll, W. *Phys. Chem. Chem. Phys.* **2008**, *10*, 7031–7038.
(44) Rowe, G. K.; Creager, S. E. *Langmuir* **1991**, *7*, 2307–2312.

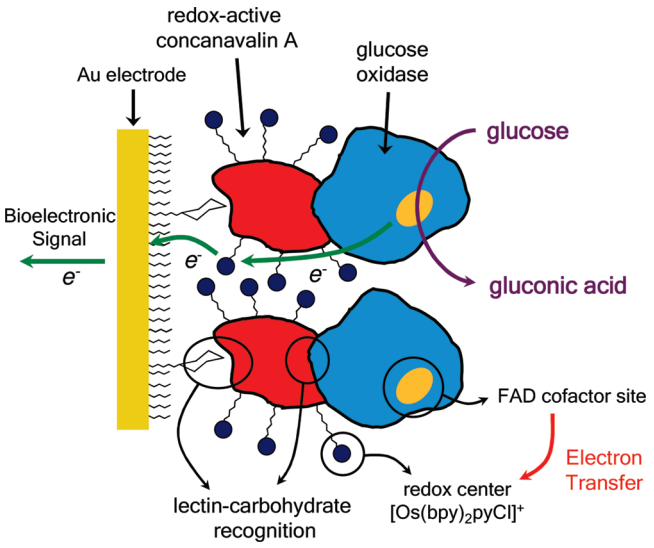

Figure 12. Illustrative schematic of the glucose-responsive interfacial supramolecular bioconjugate spontaneously assembled via molecular recognition processes. The figure describes the constituting building blocks participating in the generation of the bioelectronic signal in the presence of glucose.

Recognition-Directed Assembly of Functional Bioelectrochemical Interfaces. It has been demonstrated that recognition-directed supramolecular assembly on Con A-modified surfaces allows the facile immobilization of glycoenzymes.[45] The carbohydrate regions in the glycoenzyme are generally located in areas that are not involved in enzyme activity, and therefore, they can retain most of their biological function even when their carbohydrate regions are conjugated on the Con A layer.[45] In the case of redox-tagged Con A, the lectin layer would act as a functional bioaffinity building block facilitating the immobilization of the enzyme and serving to electrically connect the redox centers of the enzymes to electrodes, without requiring the use of electron-shuttling diffusional redox mediators in solution. Moreover, owing to its tetravalent nature Con A is also able to form multilayers via successive recognition-directed assembly of the lectin and the glycoprotein.[46] To illustrate this redox-biosupramolecular concept, we have chosen glucose oxidase, which has been intensively used for the construction of chemical-responsive bioelectronic interfaces, as a model glycoenzyme to be assembled and wired onto the redox-tagged Con A-modified electrode (Figure 12).

Mannosylated gold electrodes were modified through the sequential recognition-directed assembly of $[Os(bpy)_2Clpy]^+$-$PEG)_{12}$-Con A and GOx. This procedure led to the construction of electrodes modified with (Os-Con A)$_1$(GOx)$_1$ and (Os-Con A)$_2$(GOx)$_2$ assemblies. To quantify the amount of glycoenzyme incoporated into the interfacial bioconjugate, we monitored the sequential immobilization process using SPR as was previously described for Os-Con A modified electrodes. These reflectivity shifts were correlated to mass coverage as indicated in Table 5. Notably, Con A modified with 12 redox centers retains its ability to bind not only the mannose groups on the electrode surface but the glycosidic portion of the enzyme as well. This behavior is fundamental for the construction of multilayered assemblies and represents a desirable feature in the development of biohybrid building blocks.

(45) Saleemuddin, M.; Husain, Q. *Enzyme Microb. Technol.* **1991**, *13*, 290–295.
(46) Cassier, T.; Lowack, K.; Decher, G. *Supramol. Sci.* **1998**, *5*, 309–315. (b) Lvov, Y.; Ariga, K.; Ichinise, I.; Kunitake, T. *J. Chem. Soc., Chem. Commun.* **1995**, 2313–2315.

Table 5. Surface Coverages of $[Os(bpy)_2Clpy]^+$-$PEG)_{12}$-Con A ($\Gamma_{Os\text{-}Con\ A}$) and Glucose Oxidase ($\Gamma_{GOx}$) as Determined by Surface Plasmon Resonance (SPR) Spectroscopy[a]

assembly (Os-Con A)$_n$ (GOx)$_n$	$\Gamma^n_{Os\text{-}ConA} \times 10^{12}$ (mol/cm^2)	$\Gamma^n_{GOx} \times 10^{12}$ (mol/cm^2)	$\Gamma^T_{Os\text{-}Con\ A} \times 10^{12}$ (mol/cm^2)	$\Gamma^T_{GOx} \times 10^{12}$ (mol/cm^2)
$n = 1$	1.88	0.87	1.88	0.87
$n = 2$	2.09	0.64	3.97	1.51

[a] Superindexes n and T denotes the protein incorporated in the n layer and the total amount of protein assembled on the electrode surface, respectively.

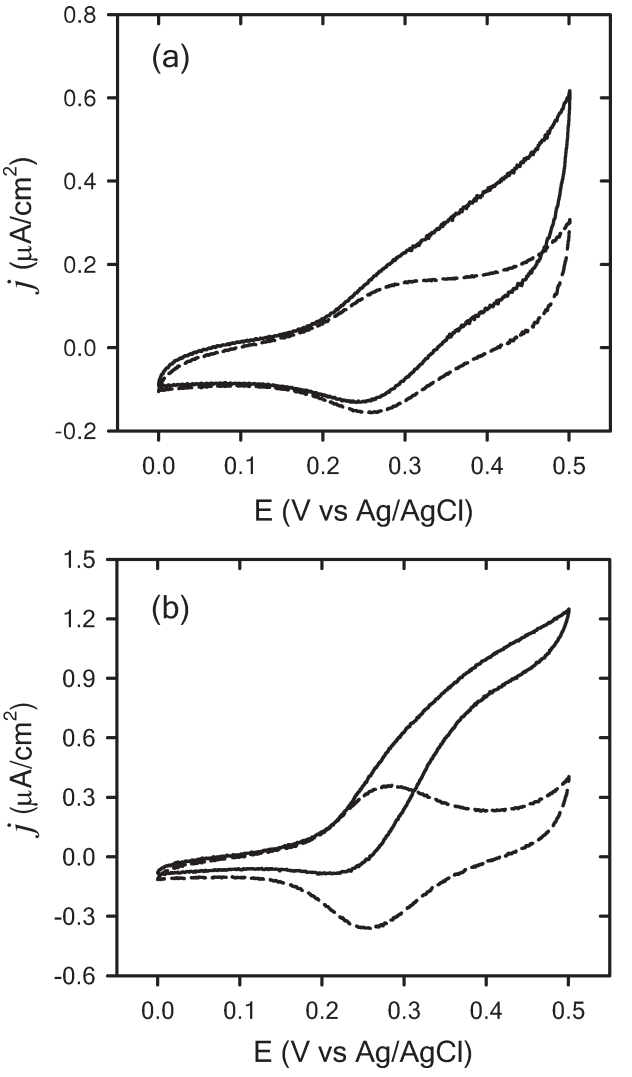

Figure 13. Cyclic voltammograms describing the electrochemical response of (a) (Os-Con A)$_1$(GOx)$_1$ and (b) (Os-Con A)$_2$(GOx)$_2$ in the absence (dashed line) and in the presence of 50 mM glucose (solid line) under argon atmosphere. $v = 5$ mV/s. $T = 298$ K. The term "Os-Con A" refers to $(Os(bpy)_2Clpy]^+$-$PEG)_{12}$-Con A. In all experiments, argon bubbling was used to remove dissolved oxygen from the measurement solutions for at least 45 min before use and for 15 min between successive measurements.

After corroborating the successful multilayered growth of redox-tagged Con A-GOx assemblies, we examined another key feature desired in these blocks: their ability for electrical communication. For this purpose, we studied their electrocatalytic behavior in the presence of the enzyme substrate. Figure 13 describes the cyclic voltammograms corresponding to (Os-Con A)$_1$(GOx)$_1$ and (Os-Con A)$_2$(GOx)$_2$ assemblies in the presence of

glucose in solution. The linear sweep voltammograms of both interfacial architectures from 0.0 to 0.5 V (vs Ag/AgCl) reveals well-defined catalytic responses of the biosupramolecular electrode in the presence of substrate compared with the background current without glucose.

The catalytic current results from oxidation at the electrode surface of $[Os(bpy)_2Clpy]^+$ to $[Os(bpy)_2Clpy]^{2+}$ as a result of a reductive neighborhood of GOx molecules. The enzyme is responsible for the catalytic oxidation of glucose to gluconic acid. The electrons generated in this reaction are transferred to the oxidized form of the artificial mediator, and thus, a catalytic current is produced. The voltammetric observation clearly verified the electrical connectivity of the enzyme with the osmium complex which acts as electron shuttle between the Au electrode and the prosthetic $FADH_2$ group in the enzyme immobilized on the Os-Con A layer. Furthermore, Figure 13 also reveals that the presence of a second Os-ConA/GOx bilayer leads not only to an increase in bioelectrocatalytic activity, but also to a better defined voltammetric response of the redox labels. This fact strongly suggests that the incorporation of the second Os-Con A layer leads to the appearance of percolation effects, thus promoting better connectivity between the redox centers in the interfacial architecture and the gold electrode. To confirm that the catalytic current was due to electron transfer between the enzyme and the osmium complex, and not to the possible presence of O_2, we performed control experiments. In these experiments, where unlabeled Con A and GOx were immobilized onto a Au electrode, no catalytic behavior was observed when slow rate cyclic voltammetry was conducted in the presence of 0.05 M glucose.

Conclusions

We described here the functionalization of Con A, a versatile protein with the ability to biorecognize carbohydrates and form glycoconjugates, with redox mediators. The approach is based on the decoration of Con A with electroactive $[Os(bpy)_2Clpy]^+$ moieties which are noted for a variety of distinctive features, including stability in aqueous aerobic media, accessibility of a large variety of derivatives, and favorable electrochemical properties. The incorporation of the electroactive groups was accomplished via chemical coupling of COOH-terminated redox centers to the peripheral lysine groups of the protein. This methodology enabled the facile synthesis of a unique set of bioinorganic building blocks bearing different amounts of redox centers, as determined by MALDI-TOF-MS. Surface plasmon resonance studies were performed in order to assess the impact of the redox tagging on the molecular recognition properties of Con A. These studies revealed that redox-tagged Con As exhibit similar immobilization behavior to that of native Con A. This indicates that neither the chemical modification of the peripheral lysine groups nor the incorporation of relatively bulky organometallic centers affects the recognition properties of the lectin. On the other hand, steady-state fluorescence studies showed a marked quenching effect of the Os centers on the intrinsic tryptophan fluorescence. This is due to the fact that the outermost Trp residues in Con A are in close proximity to the peripheral reactive Lys groups, which participate in the covalent binding of the redox centers. Structural analysis performed by small-angle X-ray scattering (SAXS) in buffered solutions corroborated the globular conformation of native tetrameric Con A in aqueous environments. The estimated dimensions were comparable to that obtained from crystallographic data. Along these lines, SAXS studies also revealed that redox-tagged Con A proteins exhibit some aggregation effects upon modification, thus leading to the formation of small aggregates (dimers or trimers) as indicated by light scattering studies. These studies also indicated that proteins modified with aminocaprilic linkers are prone to aggregation, while those modified with PEG linkers display better colloidal stability, even if they are heavily modified with Os centers. This experimental observation reinforces the idea that the nature of the linker plays a key role in the colloidal stability of the biohybrid building blocks. Electrochemical studies showed the redox-active properties of the hybrid building block when assembled on Au electrodes via a sugar-lectin recognition-directed process. Comparison of the entire population of redox centers, as determined by SPR, and its corresponding active population, as determined by cyclic voltammetry, revealed that only a fraction of the $[Os(bpy)_2Clpy]^+$ sites are connected to the electrode support. Even though not all the redox sites in the supramolecular conjugate are wired to the electrode, the magnitude of the electrochemical response is proportional to the average number of Os centers incorporated on each Con A molecule. Furthermore, differential-pulse voltammetry experiments provided evidence to corroborate that the nature of the linker affects the redox potential of the electroactive moeties. This has been attributed to the fact that PEG and aminooctanoic linkers introduce different solvent environments which, in turn, have an impact on the stability of the redox couples.

Then, we demonstrated the integration/connection of GOx to electrodes via bioaffinity interactions. Recognition-directed assembly of the glycoenzyme on the redox-active affinity layer through lectin−carbohydrate interactions resulted in a functional biprotein assembly displaying a remarkable electrochemical responsiveness to the presence of substrate in solution. The implementation of simple synthetic protocols and well-established biophysical characterization tools demonstrates how the interplay between organometallic chemistry and biology can still offer novel designs for functional biomolecules capable of evolving as elemental tools for the development of new and interesting bioelectronic platforms in the near future.

Acknowledgment. The authors acknowledge financial support from Max-Planck-Gesellschaft (Max Planck Partner Group for Functional Supramolecular Bioconjugates, MPIP-INIFTA), Consejo Nacional de Investigaciones Científicas y Técnicas (CONICET) (PIP 2009-0362) Agencia Nacional de Promoción Científica y Tecnológica (BID PICT 00575 y PAE 2006 37063 − PRH 2007 No. 74 − PIDRI No. 74 − PICT 163/08), Centro Interdisciplinario de Nanociencia y Nanotecnología (CINN − ANPCyT − Argentina), Alexander von Humbolt Stiftung (Germany) and Laboratório Nacional de Luz Síncrotron (LNLS − Brazil). D.P acknowledges CONICET for a postdoctoral fellowship. M.C., F.B., and O.A. are CONICET fellows. M.C. is a Full Professor at the Universidad Nacional del Noroeste de Buenos Aires.

Supporting Information Available: Characterization of the redox-active linkers by laser desorption mass spectroscopy, control experiments performed on Con A subjected to the same coupling conditions used to conjugate the redox centers, MALDI-TOF mass spectra of $([Os(bpy)_2Clpy]\text{-}PEG)_{12}$-Con A, surface plasmon resonance (SPR) characterization of the immobilization of redox-tagged Con A on mannosylated gold surfaces and cyclic voltammetry experiments at high scan rates. This material is available free of charge via the Internet at http://pubs.acs.org.